Photophysics and photochemistry of functionalized anthradithiophene in microcavities

Winston T. Goldthwaite[a], Roshell Lamug[a], Jonathan D. B. Van Schenck[a], Richard Puro[a], John E. Anthony[b], and Oksana Ostroverkhova[a]

[a]Department of Physics, Oregon State University, Corvallis, OR 97331
[b]Department of Chemistry, University of Kentucky, Lexington, KY 40506

ABSTRACT

We present a study of photodegradation in functionalized anthraditiophene (diF TES-ADT)-based films in hybrid cavities composed of distributed Bragg reflector (DBR) bottom mirror and top silver (Ag) mirror, depending on two different DBR reflectivity stopbands. The concentration of diF TES-ADT was chosen such that the films contain molecules in "amorphous" and "aggregate" phases characterized by different optical absorption spectra. We demonstrate that the cavity photon preferentially couples to the molecules in the "amorphous" phase and observe different photodegradation, attributed to photodimerization, dynamics for cavity photon-coupled and uncoupled states. The presence of the longer lived emissive states, such as entangled triplet pair (TT) states formed in the process of singlet fission, was correlated with a faster photodimerization dynamics. The observed cavity-dependent photodimerization dynamics offers an opportunity to manipulate the reaction rates and yield with cavity characteristics.

Keywords: Organic semiconductors, photodimerization, exciton polaritons

1. INTRODUCTION

Organic (opto)electronic materials have attracted attention due to their low-cost, solution processability, and tunable properties;[1] applications including thin-film transistors, solar cells, light-emitting diodes, and sensors have been demonstrated.[2] One of the areas utilizing organic functional materials that has experienced dramatic growth is polariton formation in organic microcavities, and associated physics and applications of this phenomenon.[3–5] These include polariton lasing, nonlinear polariton–polariton interactions, polariton electroluminescence, and polariton Bose–Einstein condensation.[4–7] It has been of considerable interest to understand how strong exciton-photon coupling, and the resulting light-matter hybrid polariton states, may contribute to the performance of organic (opto)electronic devices.[8–12] In order to efficiently utilize strong exciton–photon coupling in enhancing device performance, it is necessary to understand the photophysics of exciton–polaritons in organic electronic materials depending on various molecular properties and microcavity configurations.

Another important aspect of optoelectronic devices development is their stability with respect to environmental factors. Recent advances in polariton chemistry[13] offer promises that photochemical reactions responsible for organic device degradation could be manipulated, and possibly delayed or prevented, using strong coupling between the molecular excitation and cavity photon.[7,14] However, the reaction rates could also be increased by molecular interactions with cavity photon,[15] and therefore it is important to understand how the photophysics of the organic material in the microcavity determines the effect of the polariton formation on photochemical processes.

Towards this goal, for our present study, we chose a benchmark organic semiconductor diF TES-ADT (Figure 1(a)) which has served as a model system for a variety of studies focusing on its performance in field-effect transistors,[1] photoconductivity,[16,17] singlet fission properties,[18–20] and strong exciton-photon coupling in microcavities.[21] In our previous study of diF TES-ADT films in all-metal microcavities, Rabi splittings of up to 340 meV were observed and an interesting trend that the cavity photon coupled to a specific molecular population

Further author information: (Send correspondence to O.O.)
E-mail: oksana@science.oregonstate.edu, Telephone: 1 541 737 1679

(which was also recently reported in TIPS-pentacene films[22]) was revealed.[21] While all-metal cavities have been successful in achieving high Rabi splittings, higher Q-factors would be desirable, for example, for understanding ultrafast exciton and polariton dynamics and for the observation of interactions leading to the polariton Bose-Einstein condensate formation. Additionally, processes at metal-organic interfaces could confound the picture. Therefore, cavities with distributed Bragg reflectors (DBRs) are of interest. For our first study utilizing DBR-based cavity structures with diF TES-ADT, we chose a hybrid cavity composed of a metal and a DBR (Figure 1(b)) and investigated selected aspects of photophysics and photochemistry involved in fabricating diF TES-ADT devices with the DBR structures and optical properties of such devices.

2. EXPERIMENTAL

2.1 Materials and Sample Preparation

In our experiments, we used blends of fluorinated anthradithiophene (ADT) derivative with a functionalized side group of (triethylsilyl)ehynyl (TES) with poly(methyl methacrylate) (PMMA). A 30 mg/mL toluene solution of PMMA was combined with diF TES-ADT at various concentrations (5.1 x 10^{-3} - 8.0 x 10^{-2} M) to create films with average diF TES-ADT molecular spacing (d) ranging from 1 to 2.5 nm. Spin-cast films will be referred to in accordance with their average molecular spacing, F_d.[21,22] At high diF TES-ADT concentrations, with $d \leq 1$ nm, optical properties of films are dominated by those of "aggregates" characterized by spectral features red-shifted (i.e. at ≥ 550 nm in the absorption spectra) from those of non-interacting molecules in dilute solution. In the $1.5 \leq d < 2.5$ nm range, spectral features of aggregates coexist with those of molecules exhibiting solution-like spectra which will be referred to as an "amorphous" phase. In dilute samples, $d \geq 2.5$ nm, the diF TES-ADT molecules are predominantly in the "amorphous" phase. The molecular structure of diF TES-ADT and its optical properties for films with different average molecular spacing are shown in Figure 1(a).

Towards fabrication of all-DBR cavities, which involve sputtering of alternating TiO_2/SiO_2 layers, we investigated the stability of diF TES-ADT with respect to sputtering requiring oxygen plasma. To study the sputtering-induced degradation of diF TES-ADT as a function of average molecular spacing, diF TES-ADT:PMMA control films with $d = 1$, 1.5, and 2.5 nm were deposited on a glass substrate with 45 nm of thermally evaporated Ag. To investigate the effectiveness and properties (such as minimum thickness) of a protective layer for oxygen plasma depositions, 10-50 nm of Al_2O_3 fabricated by atomic layer deposition was added on top of another set of diF TES-ADT:PMMA/Ag/glass films (inset of Fig. 2(b)). The control and protected samples were then finished by depositing 60 nm of SiO_2 by sputter deposition resulting in structures shown in the insets of Figs. 2(a) and (b)).

For studies of photodegradation in optical cavities, we fabricated two hybrid (Ag top and DBR bottom mirrors) cavities designed with two different center reflectivities. Schematic of the cavity is shown in Fig. 1(b). The hybrid cavities were configured with 10.5 pairs of TiO_2/SiO_2 as bottom DBRs produced by sputter deposition. The thicknesses of the alternating TiO_2 and SiO_2 layers were set to be $\lambda_0/4n$, where λ_0 is the center wavelength of the DBR stop band, and n is the refractive index of TiO_2 or SiO_2 at the center wavelength, $\lambda_0 = 558$ nm or $\lambda_0 = 582$ nm. DiF TES-ADT:PMMA films were spin-cast from toluene solution to deposit a film with average diF TES-ADT molecular spacing of d = 1.5 nm ($F_{1.5}$) and a film thickness of 98 nm (measured by atomic force microscopy). Control samples, with PMMA-only films in the same cavity structures, were also fabricated. The cavity was finished by depositing a 45 nm Ag top mirror. A top-mirror configuration of Ag (45 nm)/diF TES-ADT/glass, which will be referred to as "top", was fabricated as a control sample.[15] Cavities will be referred to by their DBR center wavelength, i.e. "558 nm" or "582 nm" cavities.

2.2 Measurements

In all samples, reflectance and photoluminescence (PL) was measured using a vertical, custom-built optical assembly mounted to an inverted microscope (Olympus IX-71). For reflectance, white light from a fiber-coupled tungsten filament source (Ocean Optics LS-1) was used to illuminate samples at normal incidence from the top side (through the SiO_2 film in samples for study of degradation due to sputtering in Fig. 2) or the Ag top mirror in hybrid cavity and top samples of Fig. 1(c)). Reflected light was then detected via fiber-optic cable using an Ocean Optics USB2000-FLG spectrometer. PL spectra were measured under 532 nm continuous wave (cw) excitation from a Verdi-5 laser (Coherent, Inc.) focused by a 10× microscope objective.

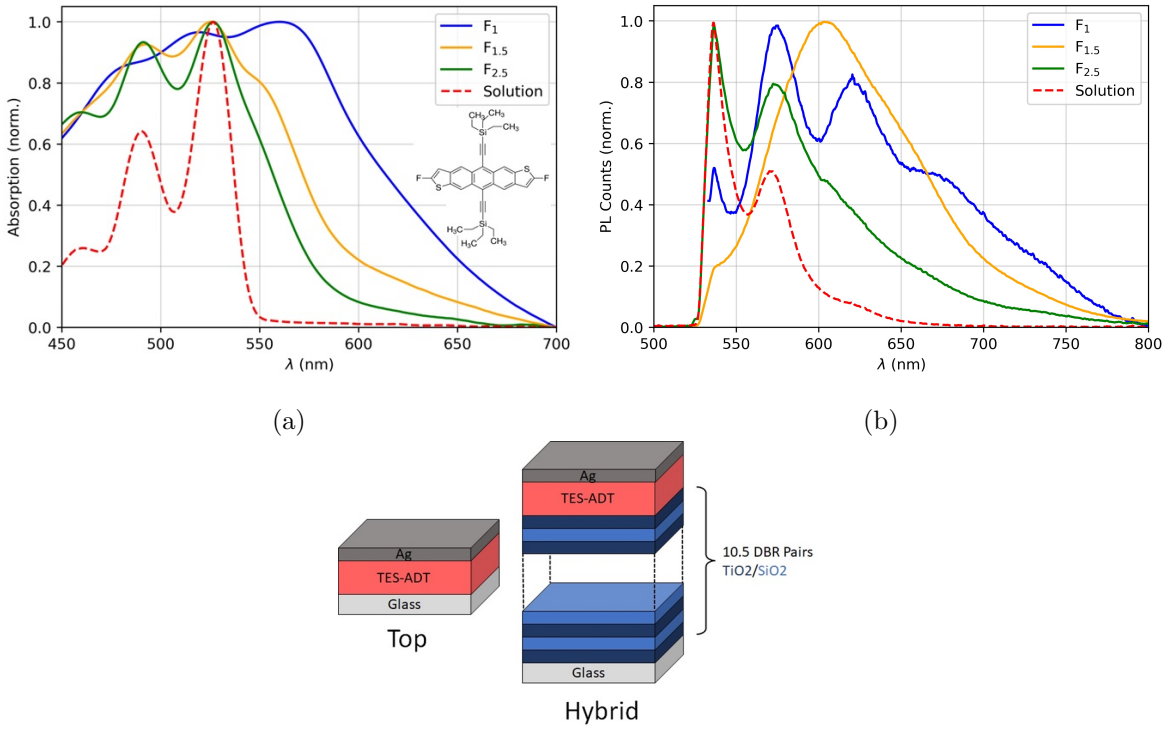

Figure 1: (**a**) Absorption and (**b**) photoluminescence (PL) of diF TES-ADT:PMMA films F_1, $F_{1.5}$, $F_{2.5}$, and solution with 532 nm cw excitation. The excitation laser filtered using a 532 nm long-pass filter which partially cuts off the spectra. Inset of (**a**) shows the molecular structure of diF TES-ADT. (**c**) Schematic of "hybrid" optical planar microcavities used. Configuration of top sample used as a control is also shown.

Angle-resolved reflectance (ARR) for all cavities, illuminated by s-polarized light at angles of incidence between 15° and 65° in 5° steps, was measured using a custom built optical assembly. White light from a fiber-coupled tungsten filament source was passed through a linear polarizer before being focused onto the sample at different angles of incidence. Reflected light was then collected and analyzed using an Ocean Optics USB2000-FLG spectrometer. The center energies of the cavity reflection resonances were modeled by using a coupled oscillators model for polaritons as described our previous publications.[21,22]

PL lifetime measurements (time-correlated single photon counting) were performed with 532 nm picosecond pulsed excitation (500 kHz frequency-doubled Nd:YAG laser, HE-1060). The emitted light was spectrally filtered to look at regions of interest, and the time-resolved PL was detected via a single-photon avalanche photodiode (SPAD, Molecular Photonic Devices) and a TCSPC (TimeHarp 200, Picoquant, Inc.). The instrument response function was measured to have a time resolution of ∼380 ps.

To induce photodegradation, cavity and top samples were irradiated using 532 nm cw excitation from a Verdi-5 laser (Coherent, Inc.) focused by a 10x microscope objective. Laser excitation for the cavities were performed through the bottom glass/DBR layer and through the Ag of the top sample at an intensity of 300 μW. The photodegradation-inducing light beam was blocked from detection with an automated beam block to periodically block excitation during PL measurements to prevent spectrometer saturation.

3. RESULTS AND DISCUSSION

3.1 Oxygen plasma-induced degradation in films during sputtering

Figure 2 shows (a) how oxygen plasma degradation of diF TES-ADT:PMMA films with different diF TES-ADT molecular spacing manifests in optical absorbance and (b) how deposition of an Al_2O_3 protective layer can prevent

deterioration. While some degradation is observed in all films, films with higher concentrations of diF TES-ADT show better stability with respect to reactions with oxygen as compared to more dilute films. This is most likely due to increased formation of aggregates and crystallites with reduced free volume, which decreases the oxygen permeability and results in inhibited reactions of diF TES-ADT with oxygen such as endoperoxide formation.[15] For example, while the F_1 film absorption shows reduction of less than 10% following SiO_2 deposition, the $F_{2.5}$ film absorption degrades by 83%. Our experiments with various thicknesses of the Al_2O_3 protective layer revealed that at least 25 nm of Al_2O_3 was needed to effectively inhibit oxygen plasma damage during the SiO_2 deposition to the films containing large populations of molecules in the "amorphous" phase such as $F_{1.5}$ and $F_{2.5}$ films. In particular, absorption reduction of 10% or less was achieved in these films when they were protected with Al_2O_3, as shown in Fig. 2(b).

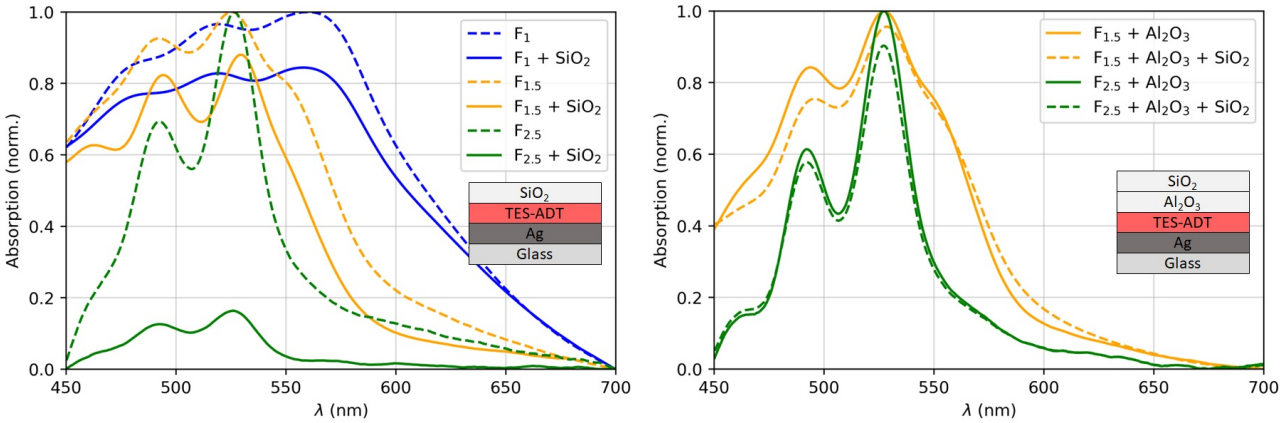

(a) (b)

Figure 2: (**a**) Normalized absorption of bare diF TES-ADT films F_1 (blue), $F_{1.5}$ (orange), and $F_{2.5}$ (green) shown in solid lines. Dashed lines show absorption of film after deposition of 60 nm SiO_2 normalized with respect to their bare film spectrum. (**b**) Normalized absorption of $F_{1.5}$ (orange), and $F_{2.5}$ (green) with added 25 nm Al_2O_3 protective layer (dashed) and 60 nm SiO_2 on top (solid). The right insets of each plot show the configuration of each sample for the associated absorption.

3.2 Optical properties of hybrid microcavities

To measure basic characteristics of the hybrid cavities, cavity Q-factors were calculated using the full width at half maximum (FWHM) of measured cavity resonances at normal incidence.[21] The reflectance under s-polarized illumination from cavities containing PMMA-only films is shown in Fig. 3(a). The 558 nm hybrid cavity yielded a Q-factor of 37, corresponding to FWHM linewidth of ∼59 meV. The 582 nm hybrid cavity yielded a Q-factor of 46, with a FWHM linewidth of ∼47 meV. Figure 3(b) shows the reflectivity stopband of the 558 nm DBR as a function of angle of incidence illuminated with either s- or p-polarized white light. With varying angle of incidence, the PMMA-only cavity resonance exhibited dispersion characteristic of that of the cavity photon, with no observed anti-crossing, confirming negligible effects of plasmon-exciton interactions from the metal-organic interface in our cavities.[23]

Figure 4 shows the reflectance and PL emission of diF TES:ADT:PMMA $F_{1.5}$ film in the two hybrid cavities discussed above at normal incidence. The optical absorption of a "bare" (i.e. outside the cavity) $F_{1.5}$ film has a mixture of the spectral features due to the contributions of the "amorphous" phase (characterized by a 0-0 transition at 2.355 eV/526 nm) and an "aggregate" phase with a 0-0 transition at ∼550 nm (Fig. 1) and their vibronic progressions.[21,22,24] In the cavities, the ARR show formation of exciton-polaritons exhibiting splitting of the spectral features (e.g. lower polariton (LP) and middle polariton (MP) at 532 nm and 518 nm, respectively, at normal incidence in the 558 nm cavity in Fig. 4(a)) and dispersive characteristics, with the coupled oscillator model fits indicating that the coupling to the cavity occurred for excited states corresponding to those of the "amorphous" phase (with the 0-0 wavelength indicated by dashed lines in Fig. 4) rather than those of the "aggregate" phase, a behavior similar to that of diF TES-ADT- and TIPS-pentacene-based films in all-metal

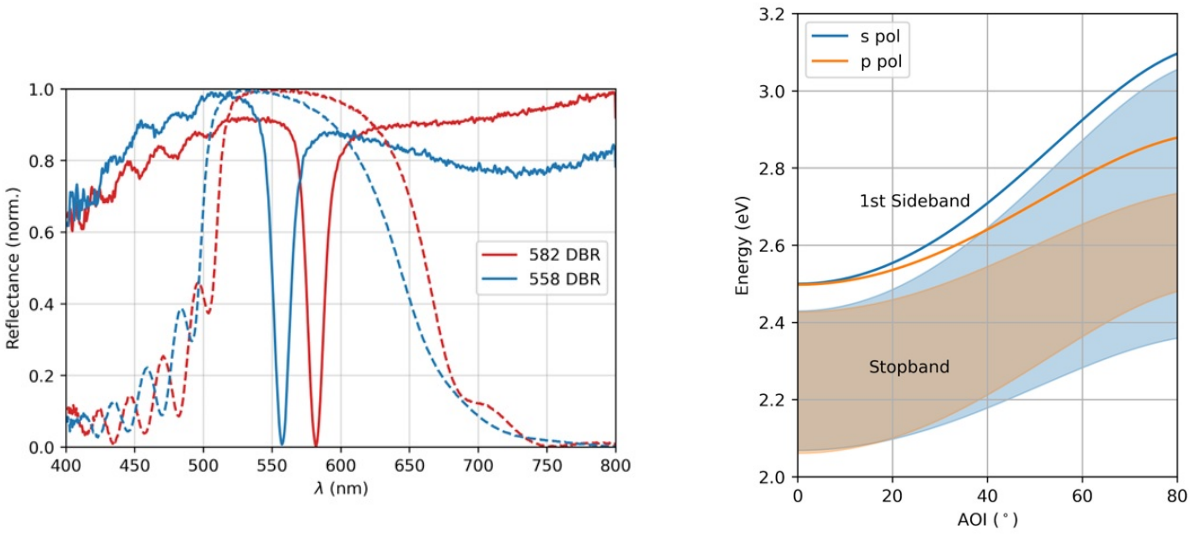

(a) (b)

Figure 3: (**a**) Reflectivity of DBR mirror (dashed) for 558 nm (blue) and 582 nm (red) DBR. Reflectance of PMMA-only film in hybrid cavity at normal incidence (solid) shows a cavity resonance at the DBR center wavelength. (**b**) DBR stopband bandwidth (shaded) and first sideband absorption peak (solid) as a function of angle of incidence (AOI) for s-polarization (blue) and p-polarization (orange) for the 558 nm DBR.

cavities.[21,22] Parameters for the coupled oscillator model fit can be found in Table 1. The exciton-photon interaction strengths $2V_{0m}$ obtained from the coupled oscillator model fits[21,22] for the 558 nm cavity yielded 33 and 51 meV for the 0-0 and 0-1 transitions, respectively, in s-polarization, and cavity detuning of 15 meV. The 582 nm cavity yielded the $2V_{0m}$ values of 33 meV and 34 meV for the 0-0 and 0-1 transitions, respectively, in s-polarization, and cavity detuning of -55 meV. The $2V_{0m}$ values are considerably lower than those of up to 150 meV obtained in similar films in all-metal cavities.[21] While some of this reduction is expected due to differences in the electric field distribution between the all-metal and hybrid cavities, further optimization of film thickness and the hybrid cavity structure is needed to enhance the interaction strength. Nevertheless, the exciton-cavity photon coupling is evident (Fig. 4(c)), enabling our studies of photodegradation in the presence of polaritons which is discussed next.

3.3 Photoluminescence from hybrid cavities

PL measurements revealed additional insights into the photophysics of films under study (Fig. 5). In both cavities, the PL emission predominantly originated from the LP branch (Fig. 4) at 532 nm in both cavities, with a minor contribution from the emission at ≥560 nm from the molecular population that is not coupled to the cavity. In the "bare" film in the control top sample, the initial PL was dominated by emission from the entangled triplet pair (TT) states (Fig. 5(c)) centered at 605 nm, with a minor contribution from S1 emission at below 600 nm (with the 0-0 emission centered at ∼535 nm). The TT states form as a result of singlet fission, which has been extensively studied in diF TES-ADT and similar materials,[18–20] and they are characterized by relatively long PL lifetimes (e.g. 13 ns in TIPS-Tc films[15]).

Insets of Fig. 5(a)-(b) show PL lifetime decays of the 558 nm (a) and 582 nm (b) hybrid cavities, measured from two different spectral regions selected by filtering the emission of the sample. The regions were selected using a 532 nm long-pass and 550 nm short-pass filters or a 600 nm long pass filter to measure specific emissive species. In particular, the region of 532-550 nm (labelled "LP") corresponds to the LP emission and the region of >600 nm (labelled "Agg") corresponds to the emission from molecular aggregates that are not coupled to the cavity. Also included in the plots is the emission from the 532-550 nm region measured in the top sample, which corresponds to the S1 emission from the "amorphous" phase with a small contribution of that from "aggregates". The lifetimes obtained from biexponential or monoexponential fits are listed in Table 2.

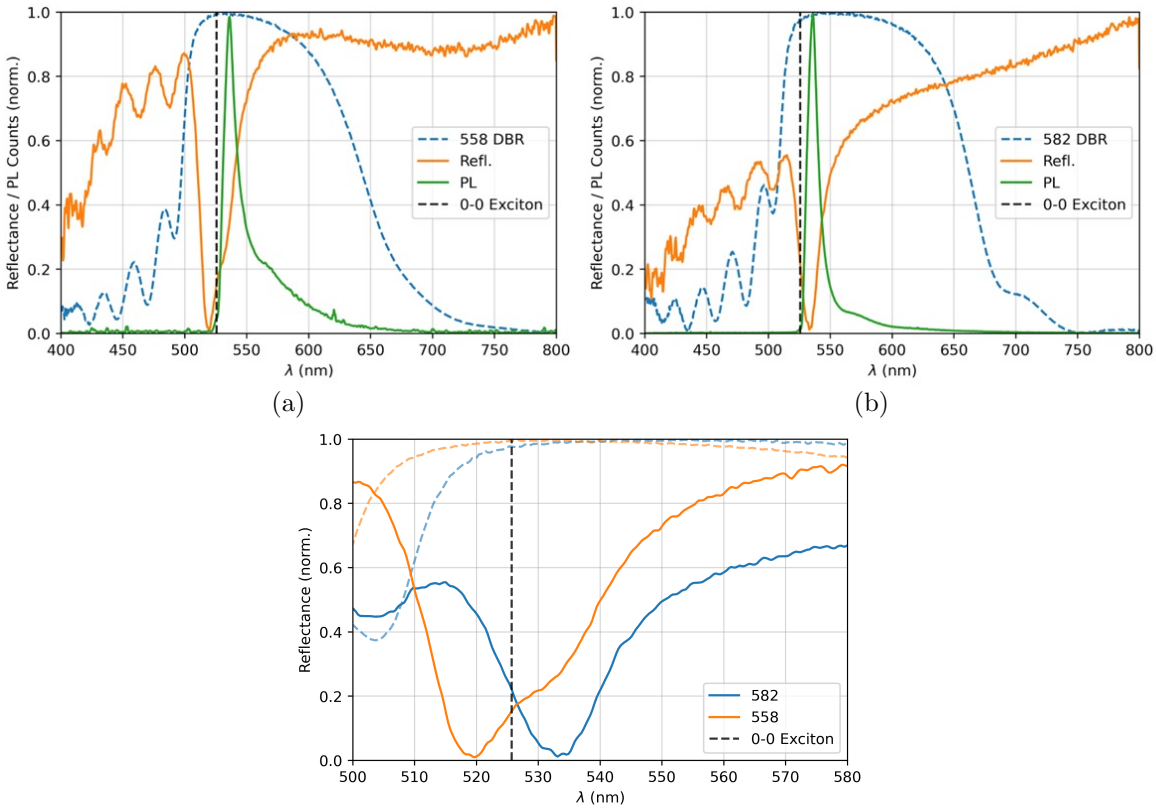

Figure 4: (**a**) Reflection (orange) and photoluminescence (green) of the diF TES-ADT:PMMA hybrid cavities at normal incidence. PL emission was filtered using a 532 nm long-pass filter. Reference reflection spectra shown for bottom DBR at normal incidence (blue, dashed) for (a) $\lambda_0 = 558$ nm and (b) $\lambda_0 = 582$ nm. The 0-0 transition energy of the "amorphous" phase of diF TES-ADT is marked at 526 nm (black, dashed). (c) Zoomed in plot of hybrid cavity reflections (solid) with corresponding bare DBR reflection spectra (dashed) at normal incidence, showing clear state splitting in the 558 nm DBR.

The data revealed two interesting observations: 1) the emission from the 558 nm cavity in both spectral regions had similar biexponential behavior to that in the S1 region of the top sample and 2) the emission from the 582 nm cavity in the region of uncoupled aggregate emission had a monoexponential decay with a lifetime of 11.8 ns consistent with that of the TT state in the "bare" film[18] whereas the LP emission had a biexponential behavior with about a factor of 2 longer lifetimes than those from the S1 region of the top sample.

Based on the Q-factors for our cavities, the cavity photon lifetime is expected to be below 100 fs, and so the long nanosecond time-scale LP lifetimes reflect the interaction between the exciton reservoir and the LP and the process of LP population.[25–27] Comparison between the lifetimes of the two cavities reveals that in the 558 nm cavity there is an effective radiative pumping of the LP from the exciton reservoir, which also suppresses formation of the TT states. In contrast, in the 582 nm cavity such pumping appears to be less efficient, possibly due to the red detuning as compared to the 558 nm cavity, which represents a bottleneck for populating the LP and promotes the TT formation instead. Next, we examine how these two scenarios affect the photodegradation process.

3.4 Photodimerization in hybrid cavities

As demonstrated in our previous work on photodegradation of functionalized tetracene (TIPS-Tc),[15] the interactions between the molecules and oxygen in cavities, which dominate the photodegradation in air, are minimal and the dominant mechanism of photodegradation in acenes and ADTs is photodimerization. Moreover, at least two

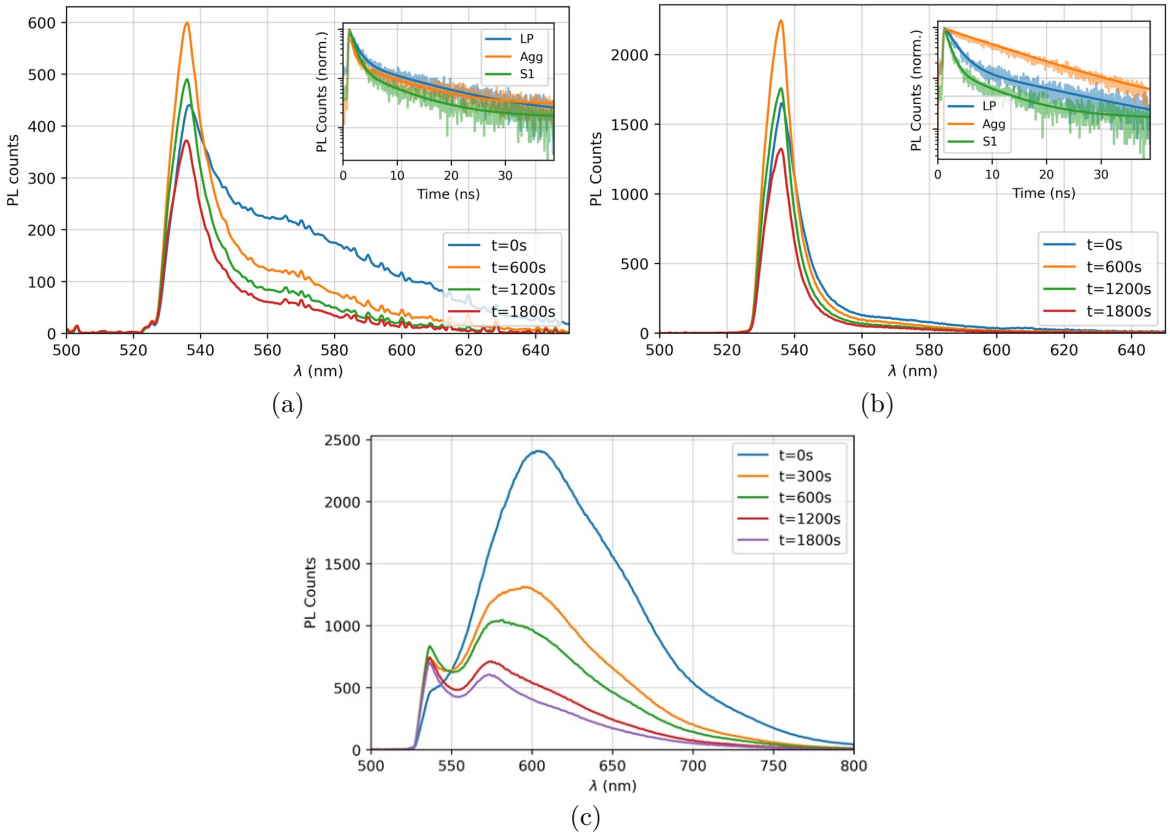

Figure 5: PL spectral evolution of (**a**) 558 nm cavity, (**b**) 582 nm cavity, and (**c**) top sample under continuous irradiation with a 532 nm cw laser over 30 minutes. Inset of (a) and (b) show PL lifetime decays of the hybrid cavities measured from the LP (532-550 nm) and uncoupled aggregate (>600 nm) spectral regions as well as S1 emission (532-550 nm) from the top sample. Fits are also included; fit parameters are listed in Table 2.

photodimerization pathways, hypothesized to be "butterfly" and alkyne dimer formation, have been identified in TIPS-Tc via formation of distinct absorption features after a prolonged illumination. We did not observe clear signatures of alkyne dimer formation in the degraded diF TES-ADT absorption spectra in the visible spectral region, and so we hypothesize that the "butterfly" dimer is the dominant reaction product.

Figures 5(a)-(c) show the PL spectral evolution upon continuous irradiation of the two cavities and the top sample with a 532 nm cw laser. For better comparison between the photodimerization dynamics in the two cavities, each PL spectrum was fitted with two Lorentzian functions corresponding to the LP and the uncoupled aggregate emission. The area of these lineshapes corresponds to the emission of the "LP" and "aggregate" regions as a function of time. The integrated LP and uncoupled aggregate emission, normalized at their values at t = 0 (fresh sample, before irradiation) and plotted as a function of irradiation time are shown in Fig. 6, illustrating a faster photodimerization process in the 582 nm cavity as compared to that in the 558 nm cavity. Similar fits with a were performed to separate the contribution of the S1 and TT states to the PL spectra of the top sample as a function of time.

Upon irradiation of the top sample, the TT emission degradation was observed, which was accompanied by an initial increase in the S1 emission that levelled off at later times and no decrease was observed during our irradiation time period (Figs. 5(c) and 6). These observations are similar to those in TIPS-Tc top samples,[15] and they suggest that once the molecular sites that have morphology conducive to the TT formation degrade, singlet fission is impeded, which promotes the S1 emission. The levelling off of the S1 emission implies that further exciton search for additional molecular sites with morphology that supports photodimerization is inefficient.

In both cavities, two distinct behaviors in the PL emission were observed: 1) an initial increase in the PL

emission from the LP state followed by decrease at later times and 2) monotonic decrease in the PL emission from the uncoupled molecular aggregates. The initial rise of the LP emission is due to the degradation of molecules in the aggregates not coupled to the cavity, which increases the molecular population that interacts with the cavity photon and populates LP. This observation illustrates the competition between the relaxation into the emissive aggregate states and the population of LP, qualitatively similar to the competition between the formation of a TT state and emission from the S1 state in the top samples.

In contrast to the levelling off of the S1 emission in the photodegradation dynamics in the top samples (Fig. 6), in both cavities the increase in the LP emission was followed by its decay which proceeded faster in the 582 nm cavity. The top sample S1 emission vs cavity LP emission differences in dynamics are consistent with the preferential coupling of molecules in the "amorphous" phase to the cavity photon discussed above, which would have a better availability of molecular sites with the morphology promoting dimerization in the "amorphous" phase as compared to the mixed "amorphous" and "aggregate" phases in the top sample. It is also possible that delocalized nature of the polariton states facilitates the search for the molecular sites favorable for dimerization, as was observed in TIPS-Tc cavities,[15] which would vary with cavity detuning and be in part responsible for the differences between the 558 nm and 582 nm cavities in Fig. 6.

The degradation dynamics of the uncoupled aggregate population in the 582 nm cavity was similar to that of the TT state in the top sample (Fig. 6), which is consistent with existence of the TT states in this cavity which are able to contribute to the leakage PL[28] as suggested by the PL lifetimes (Table 2). In the 558 nm cavity, the TT population is suppressed, which could indicate that molecules that form aggregates but have configurations not conducive to the TT formation are more stable with respect to photodimerization.

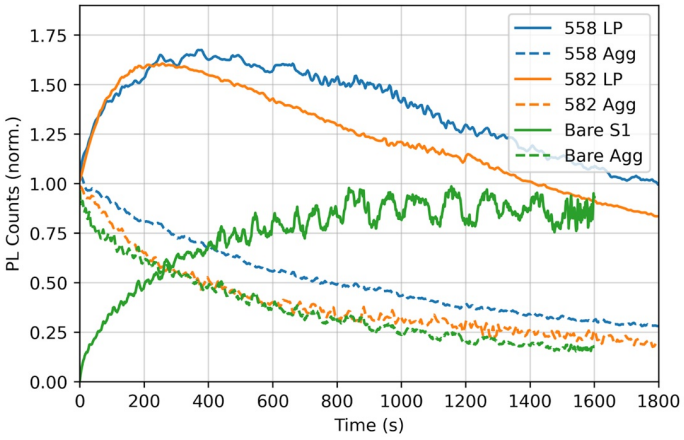

Figure 6: Integrated PL spectra versus time of the LP (solid) and aggregate (dashed) emission from the 558 nm cavity (blue) and 582 nm cavity (orange). Top ("bare") control sample integrated PL is also included (green), corresponding to "bare S1" and aggregate/TT ("Bare Agg") emission. All PL counts, except for "bare S1" are normalized at their values at t = 0.

4. CONCLUSIONS

We fabricated hybrid DBR/diF TES-ADT:PMMA/Ag cavities with two values of detuning and examined photophysics and relevant photodegradation processes in diF TES-ADT in the cavities as compared to an encapsulated "bare" diF TES-ADT:PMMA film (top sample). In mixed-phase diF TES-ADT:PMMA films that contain both the "amorphous" and "aggregated" phase molecules, the cavity photon preferentially coupled to the molecules in the "amorphous" phase. Under continuous 532 nm irradiation, degradation was observed in top samples and in cavities, which we attribute to photodimerization. The PL spectral evolution was observed during the irradiation which revealed different photodegradation dynamics of molecules responsible for emission from different states. In top samples, the molecular configurations that are conducive to the TT state formation were more vulnerable

to the dimerization. In the cavities, the "aggregate" population which is not coupled to the cavity experienced dimerization with different rates depending on detuning, with a faster rate in the cavity that exhibited more pronounced signatures of the TT states. In the "amorphous" population that couples to the cavity, the dimerization of the molecules populating LP was faster than of those responsible for the S1 emission in the top sample, with the rates depending on the cavity detuning. Our results indicate that selective coupling to the cavity and the detuning to manipulate the interactions between the exciton and polariton states could be used for controlling the rates of photochemical reactions responsible for photostability.

APPENDIX A. COUPLED OSCILLATOR MODEL PARAMETERS

Table 1: Fitting parameters for a coupled oscillator model[21] fit to angle-resolved reflectance data for the two cavities, taken as described in Section 2.2. The difference in photon energy E_0 between the two cavities can be attributed to the different stopband bandwidths, resulting in a positive detuning ($\Delta = E_0 - E_x^{(00)}$, where $E_x^{(00)}$ is the "bare" 0-0 exciton energy of 2.355 eV) for the 558 nm cavity and a negative detuning for the 582 nm cavity.

	E_0	n_{eff}	V_{00}	V_{01}	Δ
558 nm cavity	2.37 eV	1.68	16.4 meV	25.3 meV	15 meV
582 nm cavity	2.30 eV	1.69	16.6 meV	17.6 meV	-55 meV

APPENDIX B. PL LIFETIMES FIT PARAMETERS

Table 2: Fitting parameters for PL decay dynamics . The decays were fit to a monoexponential $A_1 e^{-(t-t_0)/\tau_1}$ for the 582 nm cavity aggregate emission and a biexponential for $A_1 e^{-(t-t_0)/\tau_1} + A_2 e^{-(t-t_0)/\tau_2}$ for the others. The data was normalized such that $A_1 + A_2 = 1$.

	Top	558 nm cavity		582 nm cavity	
	S1	LP	Aggregate	LP	Aggregate
τ_1 (ns)	0.99	1.29	0.65	1.99	11.76
τ_2 (ns)	7.6	11.46	8.49	16.91	-
A_1	0.82	0.81	0.80	0.84	1
A_2	0.18	0.19	0.20	0.16	-

ACKNOWLEDGMENTS

We thank V. S. Jain for the AFM measurements. This work was supported by the National Science Foundation (NSF) (Grant No. CHE-1956431). Device fabrication and characterization was made possible by the NSF MRI DMR-1920368 and NNCI:NNI EECS-2025489 awards.

REFERENCES

[1] Ostroverkhova, O., "Organic optoelectronic materials: Mechanisms and applications," *Chem. Rev.* **116**, 13279–13412 (2016).

[2] Ostroverkhova, O., [*Handbook of Organic Materials for Electronic and Photonic Devices*], Woodhead Publishing (2018 (second edition)).

[3] Holmes, R. J. and Forrest, S. R., "Strong exciton–photon coupling in organic materials," *Organic Electronics* **8**, 77–93 (2007).

[4] Sanvitto, D. and Kéna-Cohen, S., "The road towards polaritonic devices," *Nature Mater* **15**, 1061–1073 (2016).

[5] Kuehne, A. J. C. and Gather, M. C., "Organic lasers: Recent developments on materials, device geometries, and fabrication techniques," *Chem. Rev.* **116**, 12823–12864 (2016).

[6] Keeling, J. and Kéna-Cohen, S., "Bose–einstein condensation of exciton-polaritons in organic microcavities," *Annu. Rev. Phys. Chem.* **71**, 435–459 (2020).

[7] Jiang, Z., Ren, A., Yan, Y., Yao, J., and Zhao, Y. S., "Exciton-polaritons and their bose–einstein condensates in organic semiconductor microcavities," *Adv. Mater.* **34**, 2106095 (2022).

[8] Gubbin, C., Maier, S. A., and Kéna-Cohen, S., "Low-voltage polariton electroluminescence from an ultrastrongly coupled organic light-emitting diode," *Appl. Phys. Lett.* **104**, 233302 (2014).

[9] Eizner, F., Brodeur, J., Barachati, F., Sridharan, A., and Kéna-Cohen, S., "Organic photodiodes with an extended responsivity using ultrastrong light–matter coupling," *ACS Photonics* **5**, 2921–2927 (2018).

[10] Krainova, N., Grede, A. J., Tsokkou, D., Banerji, N., and Giebink, N. C., "Polaron photoconductivity in the weak and strong light-matter coupling regime," *Phys. Rev. Lett.* **124**, 177401 (2020).

[11] Wang, M., Hertzog, M., and Börjesson, K., "Polariton-assisted excitation energy channeling in organic heterojunctions," *Nat. Commun.* **12**, 1874 (2021).

[12] Nikolis, V. C., Mischok, A., Siegmund, B., Kublitski, J., Jia, X., Benduhn, J., Hörmann, U., Neher, D., Gather, M. C., Spoltore, D., and Vandewal, K., "Strong light-matter coupling for reduced photon energy losses in organic photovoltaics," *Nat. Commun.* **10**, 3706 (2019).

[13] Ribeiro, R. F., Martínez-Martínez, L. A., Du, M., Campos-Gonzalez-Angulo, J., and Yuen-Zhou, J., "Polariton chemistry: controlling molecular dynamics with optical cavities," *Chem. Sci.* **9**, 6325–6339 (2018).

[14] Peters, V., Faruk, M. O., Asane, J., Alexander, R., Peters, D. A., Prayakarao, S., Rout, S., and Noginov, M. A., "Effect of strong coupling on photodegradation of the semiconducting polymer p3ht," *Optica* **6**, 318 (2019).

[15] Puro, R., Schenck, J. D. B. V., Center, R., Holland, E. K., Anthony, J. E., and Ostroverkhova, O., "Exciton polariton-enhanced photodimerization of functionalized tetracene," *J. Phys. Chem. C* **125**, 27072–27083 (2021).

[16] Platt, A. D., Day, J., Subramanian, S., Anthony, J. E., and Ostroverkhova, O., "Optical, fluorescent, and (photo)conductive properties of high-performance functionalized pentacene and anthradithiophene derivatives," *J. Phys. Chem. C* **113**, 14006–14014 (2009).

[17] Paudel, K., Giesbers, G., Schenck, J. D. B. V., Anthony, J. E., and Ostroverkhova, O., "Molecular packing-dependent photoconductivity in functionalized anthradithiophene crystals," *J. Phys. Chem. C* **67**, 311–319 (2019).

[18] Bossanyi, D. G., Matthiesen, M., Wang, S., Smith, J. A., Kilbride, R. C., Shipp, J. D., Chekulaev, D., Holland, E., Anthony, J. E., Zaumseil, J., Musser, A. J., and Clark, J., "Emissive spin-0 triplet-pairs are a direct product of triplet–triplet annihilation in pentacene single crystals and anthradithiophene films," *Nat. Chem.* **13**, 163–171 (2021).

[19] Schenck, J. D. B. V., Mayonado, G., Anthony, J. E., Graham, M. W., and Ostroverkhova, O., "Molecular packing-dependent exciton dynamics in functionalized anthradithiophene derivatives: From solutions to crystals," *J. Phys. Chem.* **153**, 164715 (2020).

[20] Mayonado, G., Vogt, K. T., Schenck, J. D. B. V., Zhu, L., Fregoso, G., Anthony, J. E., Ostroverkhova, O., and Graham, M. W., "High-symmetry anthradithiophene molecular packing motifs promote thermally activated singlet fission," *J. Phys. Chem. C* **126**, 4433–4445 (2022).

[21] Schenck, J. D. B. V., Tanyi, E. K., Cheng, L.-J., Anthony, J., and Ostroverkhova, O., "Strong exciton–photon coupling in anthradithiophene microcavities: from isolated molecules to aggregates," *MRS Comm.* **9**, 956–963 (2019).

[22] Schenck, J. D. B. V., Goldthwaite, W. T., Puro, R., Anthony, J., and Ostroverkhova, O., "Exciton polaritons reveal "hidden" populations in functionalized pentacene films," *J. Phys. Chem. C* **125**, 27381–27393 (2021).

[23] Grant, R. T., Michetti, P., Musser, A. J., Gregoire, P., Virgili, T., Vella, E., Cavazzini, M., Georgiou, K., Galeotti, F., Clark, C., Clark, J., Silva, C., and Lidzey, D. G., "Efficient radiative pumping of polaritons in a strongly coupled microcavity by a fluorescent molecular dye," *Adv. Opt. Mater.* **10**, 1615–1623 (2016).

[24] Shepherd, W. F. B., Platt, A. D., Hofer, D., Ostroverkhova, O., Loth, M., and Anthony, J. E., "Aggregate formation and its effect on (opto)electronic properties of guest-host organic semiconductors," *Appl. Phys. Lett.* **97**, 163303 (2010).

[25] Hulkko, E., Pikker, S., Tiainen, V., Tichauer, R. H., Groenhof, G., and Toppari, J. J., "Effect of molecular stokes shift on polariton dynamics," *J. Chem. Phys.* **154**, 154303 (2021).

[26] Mony, J., Hertzog, M., Kushwaha, K., and Börjesson, K., "Angle-independent polariton emission lifetime shown by perylene hybridized to the vacuum field inside a fabry–pérot cavity," *J. Phys. Chem. C* **122**, 24917–24923 (2018).

[27] Ballarini, D., Giorgi, M. D., Gambino, S., Lerario, G., Mazzeo, M., Genco, A., Accorsi, G., Giansante, C., Colella, S., D'Agostino, S., Cazzato, P., Sanvitto, D., and Gigli, G., "Polariton-induced enhanced emission from an organic dye under the strong coupling regime," *Adv. Opt. Mater.* **2**, 1076–1081 (2014).

[28] Herrera, F. and Spano, F. C., "Dark vibronic polaritons and the spectroscopy of organic microcavities," *Phys. Rev. Lett.* **118**, 223601 (2017).